NASA TN D-436

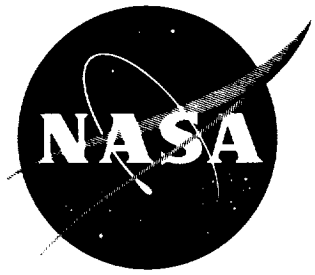

TECHNICAL NOTE
D-436

EXPERIMENTAL INVESTIGATION OF TWO LOW-DRAG SUPERCAVITATING HYDROFOILS AT SPEEDS UP TO 200 FEET PER SECOND

By Kenneth W. Christopher and Virgil E. Johnson, Jr.

Langley Research Center
Langley Field, Va.

NATIONAL AERONAUTICS AND SPACE ADMINISTRATION

WASHINGTON August 1960

NATIONAL AERONAUTICS AND SPACE ADMINISTRATION

TECHNICAL NOTE D-436

EXPERIMENTAL INVESTIGATION OF TWO LOW-DRAG SUPERCAVITATING HYDROFOILS AT SPEEDS UP TO 200 FEET PER SECOND

By Kenneth W. Christopher and Virgil E. Johnson, Jr.

SUMMARY

An experimental investigation has been made in the Langley high-speed hydrodynamics facility to determine the force and moment characteristics of two hydrofoils (one having an aspect ratio of 1 and the other having an aspect ratio of 3) designed to have improved lift-drag ratios when operating under either supercavitating or ventilated conditions. Measurements were made of lift, drag, and pitching moment over a range of angles of attack from 4° to 20° for depths of submersion varying from 0 to approximately 1 chord. The range of speed for the investigation was from 110 to 200 feet per second.

When the upper surface of the hydrofoils was completely unwetted, the experimental values of lift and drag forces were in good agreement with the theoretical values obtained from the zero-cavitation-number theory. The theoretical values for minimum angle of attack for operation with the upper surface of the hydrofoil unwetted define the lower limits of angle of attack for which the experimental values of lift coefficient are either in agreement with or slightly greater than those predicted by theory.

INTRODUCTION

Hydrodynamic lifting surfaces having supercavitating- or ventilated-flow characteristics superior to those of conventional airfoil shapes have been derived and are discussed in references 1 and 2. In reference 2, a method is presented for calculating the forces and moments on supercavitating hydrofoils of finite aspect ratio operating at various depths of submersion. A family of supercavitating-hydrofoil sections which have improved lift-drag ratios have been derived in reference 2 by assuming five terms in the vorticity-distribution expansion of the equivalent airfoil. Two of these hydrofoils, one of aspect ratio 1 and the other of aspect ratio 3, have been experimentally

investigated at speeds up to 80 feet per second. (See ref. 3.) The range of angles of attack and depths of submersion for supercavitating flow reported in reference 3 was limited by the range of speeds obtainable.

The purpose of the present investigation was to extend the range of experimental data on these two hydrofoils to higher speeds and particularly to study the characteristics of the hydrofoils at very high speeds in the range of angles of attack where the upper surface of the hydrofoil becomes wetted.

SYMBOLS

A	aspect ratio
C_L	lift coefficient, $\frac{\text{Lift}}{qS}$
C_D	drag coefficient, $\frac{\text{Drag}}{qS}$
C_{cp}	center-of-pressure coefficient, $\frac{\text{Distance from leading edge}}{\text{Chord}}$
c	chord length, ft
d/c	depth of submersion with respect to chord, measured from local mean water surface to leading edge
h	height of spray above reference line, measured perpendicular to reference line
p_c	cavity pressure, lb/sq ft
p_o	free-stream pressure at mean depth of hydrofoil, lb/sq ft
L/D	lift-drag ratio
q	free-stream dynamic pressure, $\frac{\rho V^2}{2}$, lb/sq ft
S	hydrofoil area, sq ft
V	speed, fps
x,y	coordinates

α angle of attack, deg

ρ mass density of water, slugs/cu ft

σ_c cavitation number based on cavity pressure, $\frac{p_o - p_c}{q}$

Subscripts to σ_c:

c,o indicate pressure measured on base of aspect-ratio-3 hydrofoil at midspan and aft of right strut, respectively

DESCRIPTION OF MODELS

The two supercavitating-hydrofoil models used in the present tests were the same models used for the tests reported in reference 3. A photograph and a drawing of the two hydrofoils are presented in figures 1 and 2, respectively. The hydrofoils had sections taken from a family of low-drag profiles derived by assuming five terms in the equation of vorticity-distribution expansion for the equivalent airfoil. Both hydrofoils had a projected planform area of 50 square inches. One hydrofoil had an aspect ratio of 1 and a design lift coefficient (two dimensional) of 0.393; the other hydrofoil had an aspect ratio of 3 and a design lift coefficient of 0.196. Both hydrofoils had sharp leading edges and flat upper surfaces. Struts with blunt trailing edges (parabolic section) were used for supporting the hydrofoils in order to facilitate ventilation of the cavity aft of the hydrofoils. The aspect-ratio-1 hydrofoil was mounted on a single strut as indicated in figure 2. A double strut was used for the aspect-ratio-3 hydrofoil to minimize tip deflection. (A single strut was used for the aspect-ratio-3 hydrofoil in the tests reported in ref. 3.)

A 1/4-inch brass tube was soldered to the rear of the parabolic struts for use in measuring cavity pressures. Two tubes were used on the aspect-ratio-3 hydrofoil; one measured the pressure at the midspan position and the other measured the pressure at the base of one strut.

APPARATUS AND PROCEDURE

The tests were conducted at the Langley high-speed hydrodynamics facility utilizing the temporary boom on the landing-loads carriage. The facility and its operation are described in reference 4. A photograph of the test setup is shown in figure 3.

Lift, drag, and pitching moments about the "electrical center" of the balance were measured by an electrical strain-gage balance attached to a hydraulically operated towing staff that could be raised or lowered to provide changes in depth of submersion of the model. The depth of submersion was measured from the undisturbed water surface to the leading edge of the model. The angle of attack of the hydrofoil was preset before each run with the variations due to structural deflection for the load expected being taken into account. Structural deflections were determined from calibrations made prior to the tests.

The outputs of the strain-gage balance were supplied to strip-chart recorders located on the carriage. Readings were taken at the three photographic stations (555 feet, 1,030 feet, and 1,510 feet from the start of run) at which water-level data were available. Photographs of the model were taken from above and below the water surface at the same stations. High-speed flash lamps, one located on each side of the underwater cameras, were used for lighting. A sketch of the longitudinal and transverse sections of the tank at a photographic station is shown in figure 4.

L
9
1
3

Data were obtained at three depths of submersion on most of the runs by allowing the towing staff to rise slowly during the run. The towing staff started to rise with the opening of a valve in a hydraulic line to the towing staff. The valve was automatically opened as the carriage started to move. A slide-wire, the output of which was supplied to an oscillograph on the carriage, was used for recording the rise of the towing staff.

The vertical location of the jet of spray from the leading edge of the hydrofoil was determined from photographic observation.

The variation in water level at each recording station was measured by means of a float-type instrument. The float (a hollow, bronze cylinder 1 inch in diameter and 6 inches long) was attached and fixed in height to the side of the tank; approximately one-half of the float was submerged with its axis perpendicular to the water surface. The buoyant force on the cylinder, which varied with the water level, was measured by a strain-gage pickup and recorded by an oscillograph.

A ventilation probe (fig. 3) was used on the low-trim—deep-depth runs in an attempt to facilitate the ventilation of the cavity aft of the hydrofoil. It was intended that the wake of the probe would provide a path through which air could flow into the cavity aft of the model. The pressure in the cavity was measured during each run and recorded by the oscillograph on the carriage.

ACCURACY

The accuracy of the quantities measured is estimated to be within the following limits:

Lift, lb	±25.0
Drag, lb	±15.0
Moment, lb-ft	±15.0
Angle of attack, deg	±0.10
Depth of submersion, in.	±0.10
Cavity pressure, lb/sq ft	±12.0
Speed, fps	±0.15

L
9
1
3

RESULTS AND DISCUSSION

The experimental data obtained in this investigation are presented in table I. The lift and drag data obtained with the two hydrofoils (one having an aspect ratio of 1 and the other having an aspect ratio of 3) and the corresponding theoretical values are plotted in coefficient form against depth of submersion in figures 5 and 6.

Lift Data

In the lift-coefficient plots of figures 5 and 6, the cavitation number based on the cavity pressure measured at the hydrofoil midspan is noted beside each data point. Although the cavitation numbers are not all zero, the finite cavitation numbers are small and, from figures 11 and 12 of reference 3, could be expected to give very nearly the same results as the zero-cavitation-number condition as long as the upper surface was not wetted. Since the cavity pressures were measured in the wake of the hydrofoil, it was possible to have low measured cavitation numbers while the upper surface of the hydrofoil was in a region that was subject to some higher cavitation number. This condition existed when the flow separated from the upper surface of the hydrofoil at the leading edge but the influence of the tips and struts caused the resulting cavity to collapse before reaching the trailing edge of the hydrofoil. Thus, the leading-edge cavity would not be ventilated to the atmosphere and the local cavitation number on the upper surface would be at some value higher than that in the wake of the hydrofoil. A line indicating the minimum trim-depth conditions for which the upper surface of the hydrofoils were completely unwetted, as determined from photographic data, is shown on the lift-coefficient plots. The data are in good agreement with the theory for angles of

attack above this line. For smaller angles of attack, the experimental data vary considerably from the theoretical data. For angles of attack slightly below the indicated minimum angle, especially at shallow depths, negative pressures existing in the region of high cavitation number on the top surface of the hydrofoil cause lift coefficients that are higher than those predicted by theory (e.g., the $\alpha = 6^\circ$ data for the aspect-ratio-3 hydrofoil). As the angle of attack is decreased or the depth is increased, the top-surface pressures become more positive and the lift coefficients decrease to a value less than that predicted by theory.

Drag Data

The experimental drag data have been corrected for the friction and form drag of the strut using values of spray thickness (not measured in the present tests) which were obtained from reference 3 for each hydrofoil. A correction, based on pressures measured aft of the strut, was also made for the base drag acting on the strut. For comparison with experimental data, a friction-drag-coefficient value of 0.003 was added to the theoretical drag values for the hydrofoils.

The drag coefficients for both hydrofoils tend to be higher than those predicted by theory for all angles of attack but are within 10 percent of theory when the top surface of the hydrofoil is unwetted.

Flow Characteristics

Photographs of the flow about the two hydrofoils at various depths of submersion and angles of attack are presented in figures 7 and 8. Figure 7(a) shows the aspect-ratio-1 hydrofoil operating at an angle of attack of 6° and at a fairly deep depth of submersion ($d/c = 0.8$, estimated). The depth of submersion was estimated by comparison with photographs taken during runs for which measured values of depth of submersion were available. At these conditions, the upper surface of the hydrofoil is fully wetted and cavitation occurs on the bottom surface of the hydrofoil. At the same angle of attack but at a shallow depth of submersion, the upper surface is still fully wetted although cavitation no longer appears on the bottom surface (fig. 7(b)). At an angle of attack of 9°, the upper surface is still fully wetted (figs. 7(c) and 7(d)) but at the shallower depth small bubbles of cavitation appear on the upper surface due to leading-edge vibration which indicates that the pressures on the top surface of the hydrofoil are reducing with increasing angle of attack. As the angle of attack is increased to 12° (fig. 7(e)), a region of separated flow appears on the top surface of the hydrofoil. The effects of the strut and tip vortex cause the

flow to become attached again near the trailing edge of the hydrofoil. The roughness of the separated flow is due to leading-edge vibration. Figure 7(f) shows the flow about the hydrofoil with the upper surface completely unwetted.

Similar photographs of the flow about the aspect-ratio-3 hydrofoil at various depths of submersion, angles of attack, and speeds are shown in figure 8.

Leading-edge vibration, which may not be tolerable in a practical application, was observed to occur for both hydrofoils as shown in figures 7 and 8. Although the inceptive conditions for leading-edge vibration were not analyzed, inception was noted to be governed by depth of submersion, angle of attack, and speed. No leading-edge vibration was observed for angles of attack greater than 12° for the aspect-ratio-1 hydrofoil or 14° for the aspect-ratio-3 hydrofoil. The influence of speed on leading-edge vibration may be noted in figures 8(c), (d), (e), and (f) for the aspect-ratio-3 hydrofoil at an angle of attack of 14°. In figure 8, for $\alpha = 14^{\circ}$ and $d/c \approx 0.48$, the speed of incipient leading-edge vibration is shown to be between 128 and 139 fps.

L
9
1
3

Lift-Drag Ratios

The variation of lift-drag ratio with depth of submersion for both hydrofoils is shown in figure 9. In the range of angles of attack and depths of submersion where the hydrofoil operates with its upper surface unwetted, the values of lift-drag ratio are independent of depth of submersion. The value of maximum lift-drag ratio decreased with an increase in depth of submersion. The angle at which the maximum lift-drag ratio occurred increased with increase in depth of submersion.

A direct comparison of lift-drag-ratio values for the two hydrofoils at a constant depth of submersion is shown in figure 10 along with corresponding theoretical values. The data symbols indicate faired lift-coefficient values taken from figures 5 and 6 and faired lift-drag-ratio values taken from figure 9 for a depth of submersion of 0.4 chord. The values of lift-drag ratio are plotted as a function of angle of attack in figure 10(a). This figure shows that, for equal angles of attack, both hydrofoils had about the same theoretical lift-drag ratio. Figure 10(b) shows that, for equal lift coefficients, the aspect-ratio-3 hydrofoil had a higher lift-drag ratio than the aspect-ratio-1 hydrofoil.

The agreement between theoretical and experimental lift-drag ratios is good in the supercavitating region where the upper surface is unwetted. As can be seen, the experimental lift-drag-ratio values

for the aspect-ratio-3 hydrofoil continue to increase with decreasing angle of attack to an angle much smaller than that for the aspect-ratio-1 hydrofoil. This results from two reasons: (1) The aspect-ratio-3 hydrofoil had a thinner section because of its smaller design lift coefficient and (2) for a given angle of attack, the increase in aspect ratio reduces the induced angle of attack and so results in a higher effective angle of attack and, thus, a higher spray angle. Consequently, the aspect-ratio-3 model can operate at lower geometric angles of attack with its upper surface unwetted. It may be noted also that the lift-drag ratio for the aspect-ratio-3 hydrofoil kept increasing with decrease in angle of attack to a value of $\alpha = 6^\circ$ whereas the maximum value would be expected to occur at the angle at which the top surface of the hydrofoil becomes wetted ($\alpha = 8^\circ$). The continued increase with decrease in angle of attack below the angle at which the upper surface of the hydrofoil became wetted is probably due to the previously mentioned condition which existed when negative pressures occurred on the upper surface of the hydrofoil because of insufficient upper surface ventilation.

L 9 1 3

Center of Pressure

Center-of-pressure-coefficient data for the two hydrofoils are plotted as a function of depth of submersion in figure 11. Good agreement with theory is indicated for angles of attack at which the flow separated from the leading edge.

Spray Height

The variation of experimental values of spray height with depth of submersion for both hydrofoils is presented in figure 12. The values of spray height were determined from photographs of the flow over the hydrofoil. Few data were obtained for the aspect-ratio-1 hydrofoil due to the absence of grid lines on the strut on most of the runs. A comparison of faired experimental data with theoretical spray contours is presented in figure 13. The theoretical values were calculated by the method given in reference 2. For the depths of submersion in figure 13, faired experimental data for the aspect-ratio-1 hydrofoil were obtainable only at an angle of attack of 16°. The results are in fair agreement with the theoretical spray contours. It may be noted that for an angle of attack of 12°, the experimental data indicate that the top surface of the aspect-ratio-1 hydrofoil would be wetted at a depth of submersion of 0.25 chord (fig. 12(a)) whereas theory (fig. 13(a)) predicts that the top surface of the hydrofoil would not be wetted until a depth slightly greater than 0.5 chord was reached. The experimental values of spray height may be expected to be slightly low because of the effect of the strut which causes a depression in the spanwise contour of the spray envelop as was shown in reference 5.

A comparison of experimental values of spray height with theoretical spray contours for the aspect-ratio-3 hydrofoil is given in figure 13(b). As the angle of attack is decreased, the experimental results indicate increasingly smaller values than those predicted by theory. At an angle of attack of 8°, experimental results are not in good agreement with theoretical results. According to the experimental evidence (fig. 12(b)), the upper surface of the hydrofoil becomes wetted at this angle of 8° for a depth of submersion of about 0.5 chord. However, the struts probably had a greater effect on the spray height for this hydrofoil than for the aspect-ratio-1 hydrofoil due to their spanwise position. The short cavity at the leading edge of the hydrofoil in figure 8(a) indicates that fairly large negative pressures exist near the leading edge of the hydrofoil and if the cavitation number were decreased either by an increase in speed or increase in flow ventilation, the cavity would increase in length until the flow became separated completely from the upper surface of the hydrofoil. Photographs are shown in figure 14 of the flow about the aspect-ratio-3 hydrofoil at an angle of attack of 4°. At a depth of submersion of 0.41 chord (estimated) (fig. 14(a)), the upper surface of the hydrofoil is completely wetted. The apparent distortion of the hydrofoil is caused by the refractive effects of the water surface. In figure 14(b) (d/c = 0.16, estimated), negative pressures are again evidenced by the short cavities near the leading edge of the model which indicate a tendency for the flow to separate; at a higher speed, the flow would probably separate completely from the upper surface of the hydrofoil. This observation is in agreement with the theory (fig. 13(b)) which indicates that at an angle of attack of 4° the flow will separate at a depth of submersion slightly less than $d/c = 0.5$.

Comparison With Low-Speed Data

Lift-coefficient data obtained at speeds up to 80 feet per second, reference 3, are presented in figure 15 (open symbols) along with the present data obtained at high speeds (solid symbols). The curves of the theoretically predicted lift-coefficient values are based on the assumption that the upper surface of the hydrofoil is not wetted. Fair agreement between the two sets of data is indicated where the upper surface of the hydrofoil was not wetted.

The crosshatched area in figure 15 indicates the range of angles of attack and depths of submersion in which the upper surface of the hydrofoil was at least partially wetted in the present tests. The double solid line indicates the theoretical curve of lift coefficient for minimum angle of attack plotted against depth of submersion for operation with the upper surface of the hydrofoil unwetted at zero cavitation number. All the data of reference 3 were obtained with flow

separation from the leading edge of the hydrofoil. In reference 3, the flow was caused to separate from the leading edge of the hydrofoil by inserting a probe into the flow over the hydrofoil. Once the flow was separated, it became vented to the atmosphere and remained separated on removal of the probe. As may be seen in figure 15(b), a vented flow was obtained at an angle of attack of 2° with the aspect-ratio-3 hydrofoil in reference 3. No probe was used in the present tests although a strut (cylindrical) was towed aft of the model in an attempt to ventilate the wake of the model at low angles of attack.

For the speeds investigated, zero-cavitation-number theory predicts values of the minimum angle of attack at which the hydrofoils can be operated with the upper surface unwetted that are from 0° to 4° less than those observed in the experiments. However, the experiments indicate that, if the speed were increased considerably or more air introduced to the upper surface so that zero cavitation number is more nearly attained on the upper surface, the theoretical prediction of the location of the upper cavity streamline will be adequate. As may be seen, the theory for the aspect-ratio-3 hydrofoil is in agreement with the experimental evidence shown in figure 14(b) which indicates a tendency for flow separation at $\alpha = 4^\circ$ and $d/c = 0.16$.

For angles of attack greater than the minimum angle for separated flow predicted by theory (fig. 15), the experimental values of lift coefficient obtained in the present investigation may be noted to be either greater than or in agreement with those predicted by theory. The values greater than the theoretical values are obtained when, due to the finite speeds involved and insufficient ventilation of the upper surface of the hydrofoil, the flow becomes partially attached to the upper surface of the hydrofoil although the pressures on the upper surface are still negative. As the angle of attack is decreased to below the minimum theoretical angle, the lift coefficients decrease to less than the theoretically predicted coefficients. Thus, the theoretical values for minimum angle of attack define the lower limits of angle of attack for which the experimental values of lift coefficient are either in agreement with or slightly greater than those predicted by theory.

CONCLUSIONS

Conclusions based on the results of the experimental investigation of two supercavitating hydrofoils (one having an aspect ratio of 1 and the other having an aspect ratio of 3) designed for improved lift-drag ratio may be summarized as follows:

1. The theory for predicting lift of supercavitating hydrofoils of arbitrary aspect ratio, camber, and depth of submersion at zero

cavitation number is in good agreement with experiment when the upper surface is completely unwetted.

2. The values of drag predicted by zero-cavitation-number theory are low but are within 10 percent of the experimental results for both hydrofoils when the upper surface is completely unwetted.

3. The theoretical values for minimum angle of attack for operation with the upper surface of the hydrofoil unwetted define the lower limits of angle of attack for which the experimental values of lift coefficient are either in agreement with or slightly greater than those predicted by theory.

4. Leading-edge vibration, the inception of which was governed by depth of submersion, angle of attack, and speed was observed to occur for both hydrofoils.

Langley Research Center,
National Aeronautics and Space Administration,
Langley Field, Va., May 18, 1960.

REFERENCES

1. Tulin, M. P., and Burkart, M. P.: Linearized Theory for Flows About Lifting Foils at Zero Cavitation Number. Rep. C-638, David W. Taylor Model Basin, Navy Dept., Feb. 1955.

2. Johnson, Virgil E., Jr.: The Influence of Depth of Submersion, Aspect Ratio, and Thickness on Supercavitating Hydrofoils Operating at Zero Cavitation Number. Presented at the Second Symposium on Naval Hydrod. (Washington), Aug. 1958.

3. McGehee, John R., and Johnson, Virgil E., Jr.: Hydrodynamic Characteristics of Two Low-Drag Supercavitating Hydrofoils. NASA MEMO 5-9-59L, 1959.

4. Christopher, Kenneth W.: Investigation of the Planing Lift of a Flat Plate at Speeds up to 170 Feet Per Second. NACA TN 3951, 1957.

5. Christopher, Kenneth W., and Johnson, Virgil E., Jr.: Experimental Investigation of Aspect-Ratio-1 Supercavitating Hydrofoils at Speeds up to 185 Feet Per Second. NASA TN D-187, 1959.

TABLE I.- TEST DATA

(a) Aspect-ratio-1 hydrofoil

α, deg	V, fps	d/c	C_L	C_D	C_{cp}	σ_c
20	153.89	0.629	0.394	0.126	0.509	0.072
20	140.68	.433	.391	.129	.510	.024
16	157.39	.290	.323	.086	.561	.005
16	145.38	.140	.328	.087	.550	.003
16	157.28	.508	.330	.090	.547	.015
16	143.67	.291	.326	.083	.567	.007
12	182.89	.247	.295	.053	.595	.002
12	168.65	.126	.277	.053	.615	.001
12	183.22	.957	.275	.059	.665	.003
12	168.48	.742	.287	.059	.642	.002
12	154.36	.600	.290	.063	.635	.003
9	168.82	.093	.250	.043	.618	0
9	169.03	.553	.210	.043	.711	.003
9	153.70	.375	.228	.045	.668	.001
8	157.55	.116	.223	.045	.677	.001
8	177.54	.666	.169	.043	.856	.002
8	163.10	.462	.185	.042	.798	.002
8	170.06	.665	.172	.044	.841	.035
8	155.17	.543	.187	.042	.790	.005
7	180.35	.684	.137	.041	1.006	.027
7	164.43	.547	.156	.039	.949	.014
7	175.56	.547	.153	.033	.943	.006
7	160.41	.537	.158	.033	.928	.006
7	175.77	.144	.195	.035	.763	0
6	164.19	.157	.174	.032	.849	0
6	150.08	.010	.200	.032	.758	.004

TABLE I.- TEST DATA - Continued

(b) Aspect-ratio-3 hydrofoil

α, deg	V, fps	d/c	C_L	C_D	C_{cp}	$\sigma_{c,c}$	$\sigma_{c,o}$
20	124.55	0.529	0.433	0.152	0.416	0.005	0.003
20	112.30	.142	.450	.158	.416	.004	.002
20	139.06	.313	.443	.154	.433	.002	.003
20	127.05	.076	.456	.160	.416	.002	.002
20	140.94	.034	.453	.157	.438	.001	.001
16	135.67	.291	.397	.111	.424	.003	.001
16	127.71	.669	.382	.107	.455	.006	.005
16	116.10	.603	.385	.107	.457	.006	.006
15	147.58	.431	.370	.095	.455	.003	.003
15	136.41	.448	.370	.096	.446	.003	.003
14	138.64	.473	.361	.088	.441	.006	.005
14	127.69	.485	.359	.088	.438	.005	.005
14	117.74	.553	.358	.087	.435	.005	.005
13	120.70	.411	.346	.079	.441	.004	.004
13	110.67	.434	.346	.079	.438	.005	.005
12	155.15	.110	.346	.074	.459	.003	.001
12	145.44	.634	.326	.068	.473	.004 .009	.006
12	133.53	.399	.333	.070	.468	.007	.004
10	161.13	.487	.302	.056	.463	0	.008
10	149.25	.223	.308	.057	.460	0	.015
10	150.47	.206	.305	.056	.467	.006	.006
10	169.32	.843	.302	.053	.461	.023	.025
10	155.88	.644	.298	.053	.469	.009	.009
9	165.39	.321	.297	.049	.468	.008	.008
9	151.84	.130	.301	.051	.466	.006	.006
9	171.50	.855	.298	.045	.477	.017	.020
9	157.74	.669	.289	.048	.467	.020	.013
8	150.37	.507	.310	.045	.550	.037	.035
8	137.71	.311	.295	.042	.564	.010	.007

TABLE I.- TEST DATA - Concluded

(b) Aspect-ratio-3 hydrofoil - Concluded

α, deg	V, fps	d/c	C_L	C_D	C_{cp}	$\sigma_{c,c}$	$\sigma_{c,o}$
7	176.95	0.720	0.256	0.038	0.478	0.044	0.044
7	162.39	.551	.270	.038	.479	.042	.040
7	149.51	.350	.281	.039	.501	.043	.045
7	178.52	.294	.277	.035	.501	.011	.012
7	164.44	.113	.275	.037	.503	.009	.008
7	167.65	.558	.268	.038	.497	.045	.045
7	154.90	.505	.286	.038	.485	.043	.046
7	181.00	.887	.256	.035	.494	.035	.037
7	167.56	.703	.264	.038	.492	.047	.052
7	154.54	.473	.281	.039	.479	.046	.048
6	180.89	.896	.205	.029	.553	.040	.041
6	166.48	.940	.216	.030	.538	.043	.041
6	180.99	.955	.195	.027	.562	.046	.051
6	167.38	.918	.209	.029	.546	.052	.055
6	164.71	.970	.213	.028	.542	.043	.044
6	151.07	.987	.209	.030	.510	.053	.054
6	163.16	.962	.216	.028	.533	.043	.044
6	151.89	.965	.211	.030	.516	.050	.050
6	186.99	.245	.256	.030	.526	.010	.012
6	173.45	.127	.259	.030	.505	.006	.008
6	160.78	.083	.269	.030	.499	.002	.002
6	200.80	.801	.212	.028	.540	.025	.023
6	188.49	.708	.224	.031	.557	.034	.042
6	173.75	.507	.241	.032	.535	.043	.040
5	193.08	.321	.211	.025	.573	.021	.021
5	179.81	.213	.223	.027	.285	.029	.031
5	167.04	.218	.241	.024	.513	.011	.018
5	180.48	.735	.171	.025	.642	.016	.013
5	165.23	.713	.177	.027	.615	.033	.039
5	151.60	.585	.193	.028	.530	.045	.044
5	185.02	.260	.228	.028	.364	.021	.022
5	171.49	.206	.236	.025	.544	.029	.029
5	157.79	.061	.241	.024	.524	.007	.006
4	169.91	.328	.173	.020	.662	.006	.007
4	176.58	.475	.128	.025	.833	.037	.039
4	161.11	.189	.212	.024	.625	.034	.029
4	185.26	.130	.205	.021	.589	.018	.018

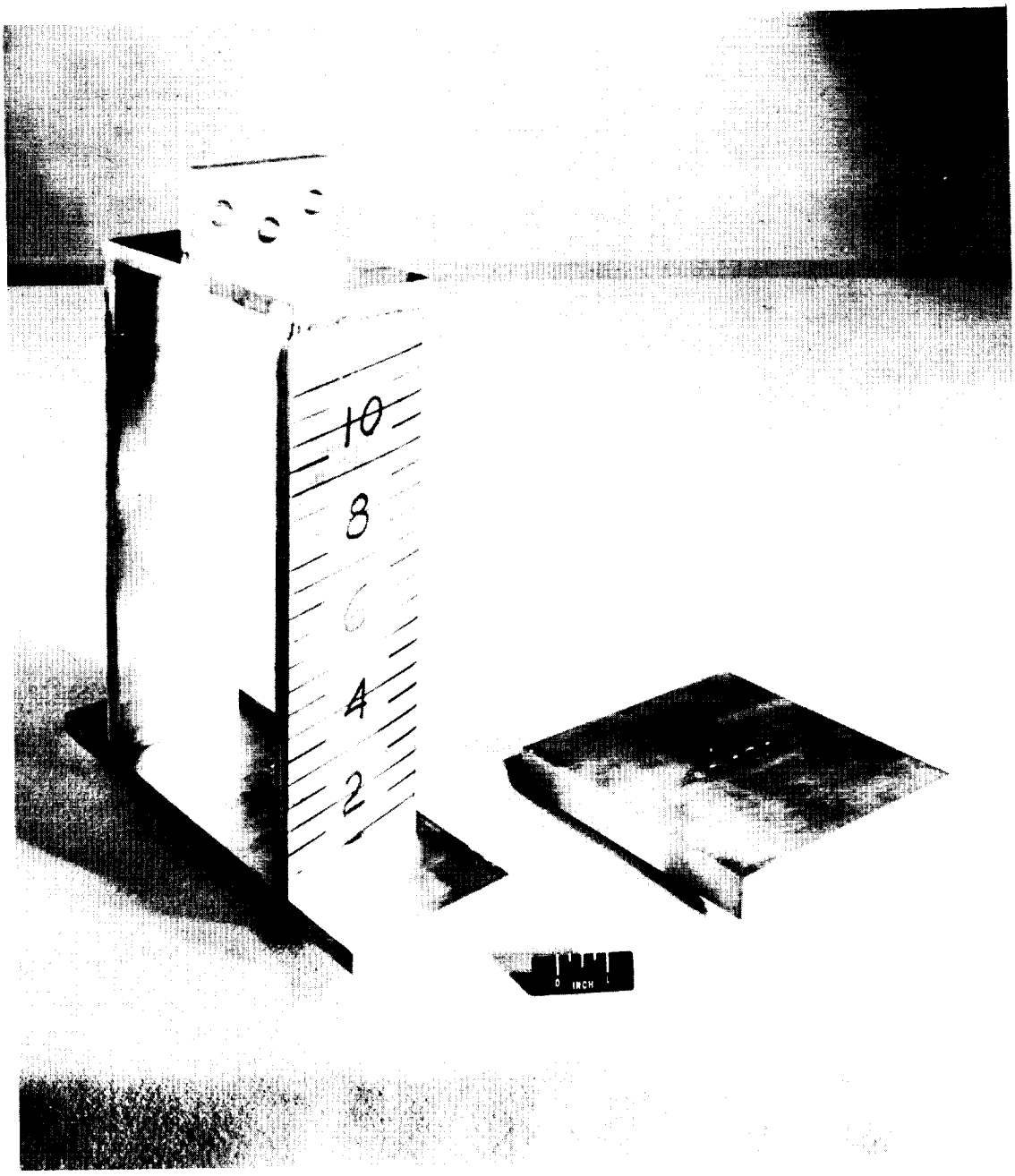

L-58-1461

Figure 1.- Photograph of the aspect-ratio-3 and aspect-ratio-1 hydrofoils.

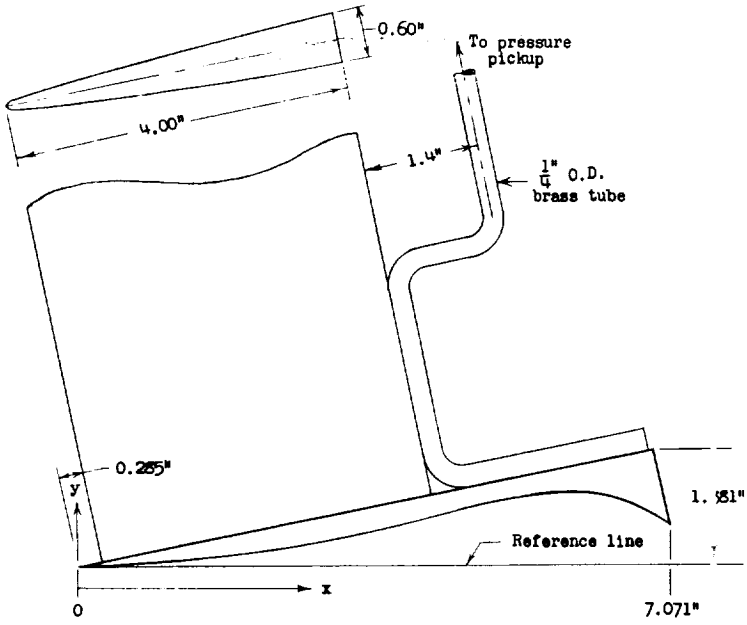

(a) Aspect-ratio-1 hydrofoil.

Bottom-surface offsets

x/c	y/c	
	A = 1	A = 3
0	0	0
.025	.0008	.0005
.050	.0018	.0010
.100	.0045	.0022
.200	.0116	.0059
.300	.0216	.0108
.350	.0281	.0142
.400	.0368	.0184
.450	.0467	.0233
.500	.0576	.0287
.550	.0694	.0348
.600	.0823	.0411
.650	.0948	.0475
.700	.1056	.0529
.750	.1144	.0573
.800	.1192	.0595
.822	.1196	.0598
.850	.1187	.0595
.900	.1110	.0556
.950	.0946	.0473
1.000	.0658	.0328

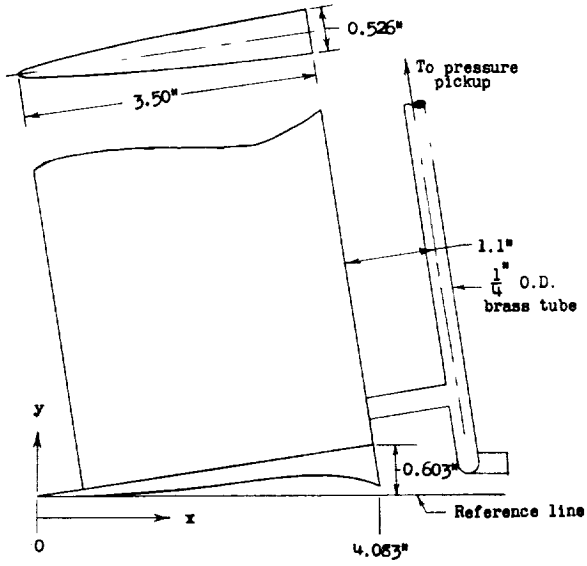

(b) Aspect-ratio-3 hydrofoil.

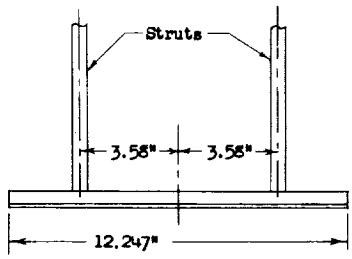

Strut locations, aspect-ratio-3 hydrofoil

Figure 2.- Drawings and offsets of the aspect-ratio-1 and aspect-ratio-3 hydrofoils.

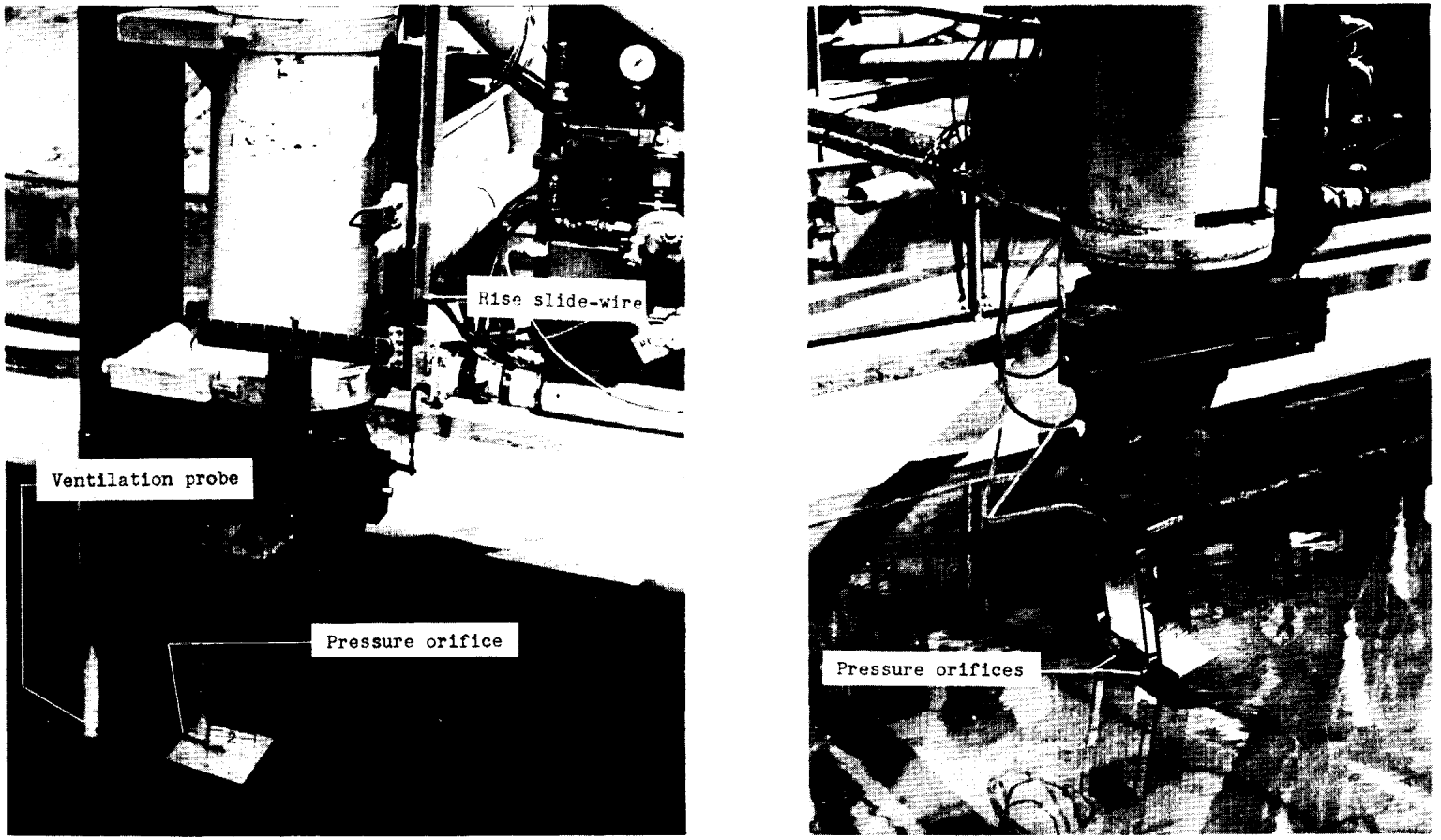

L-60-2439

(a) Aspect-ratio-1 hydrofoil.

(b) Aspect-ratio-3 hydrofoil.

Figure 3.- Photographs of test setup.

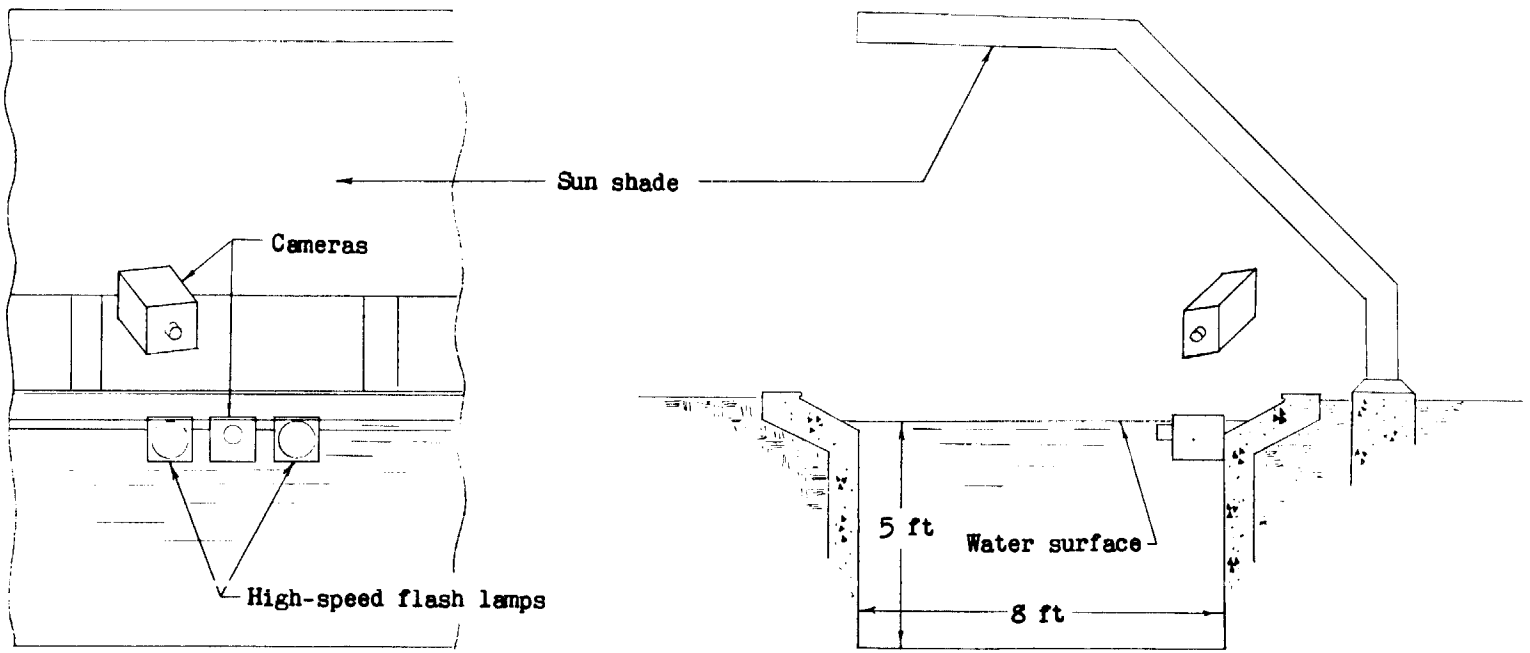

(a) Longitudinal section.

(b) Transverse section.

Figure 4.- Sections of the tank at a photographic station.

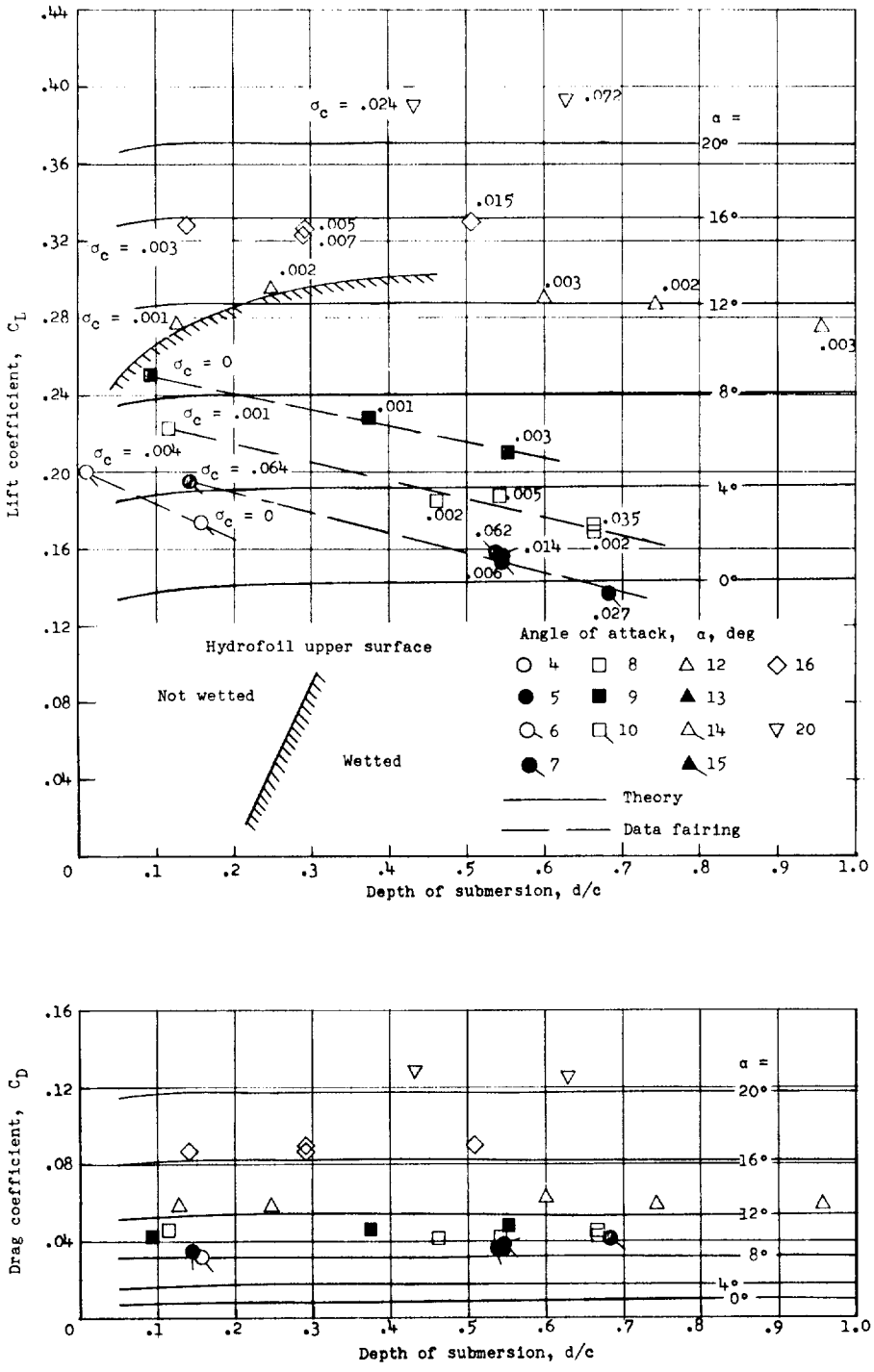

Figure 5.- Variation of lift and drag coefficients with depth of submersion for the aspect-ratio-1 hydrofoil.

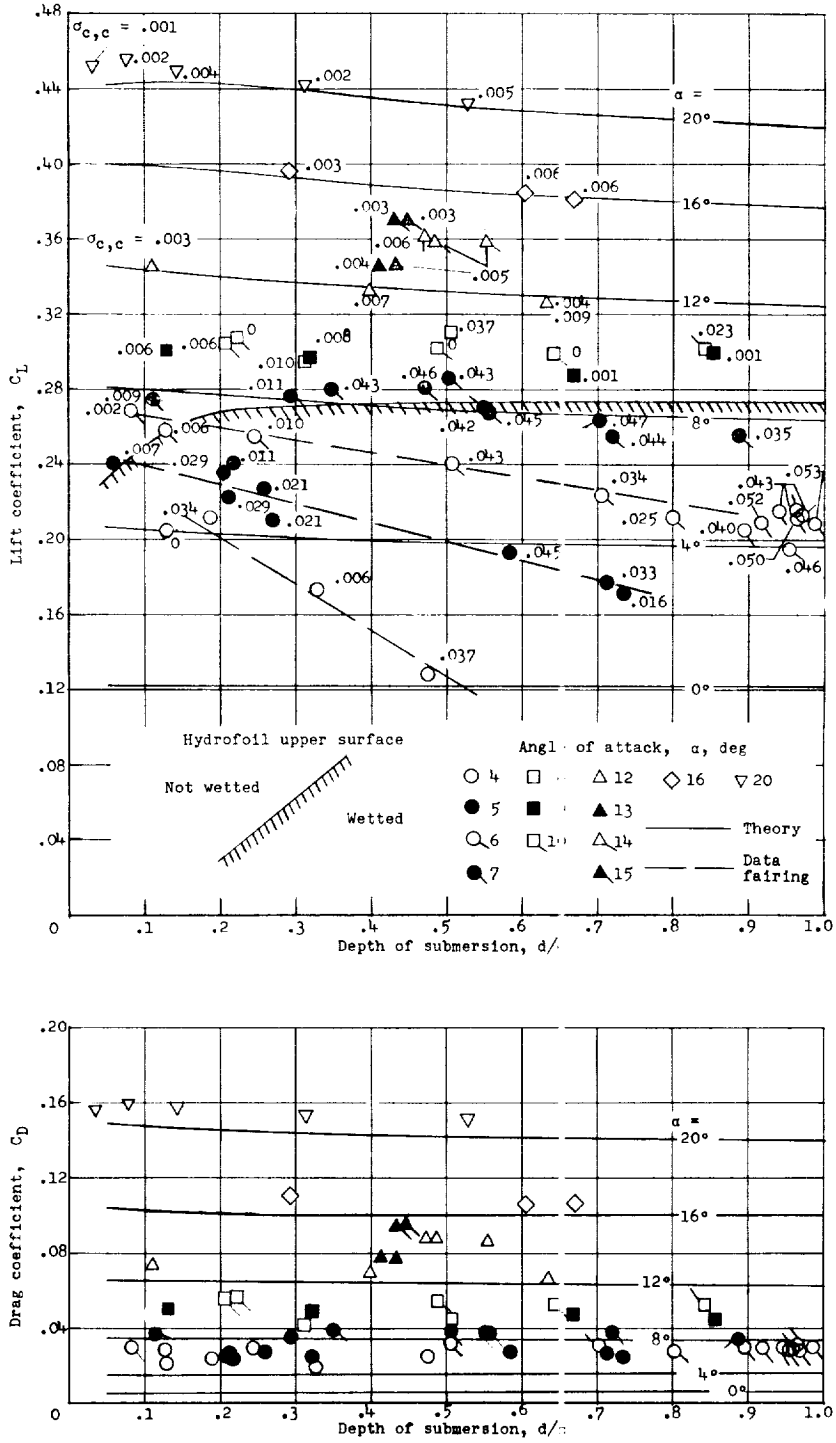

Figure 6.- Variation of lift and drag coefficients with depth of submersion for the aspect-ratio-3 hydrofoil.

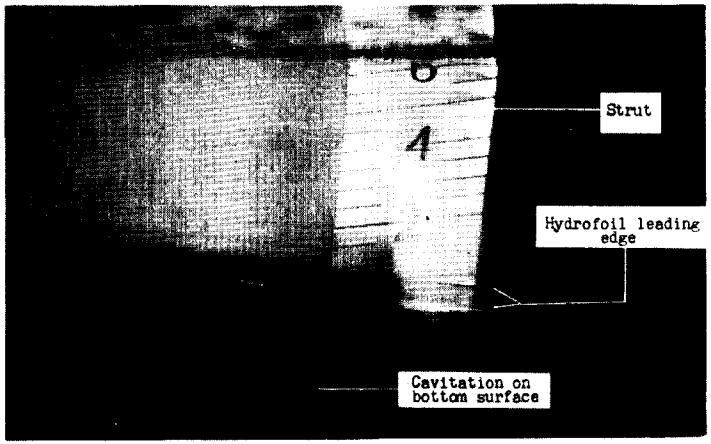

(a) $\alpha = 6^\circ$; d/c = 0.8 (estimated); V = 198.97 fps.

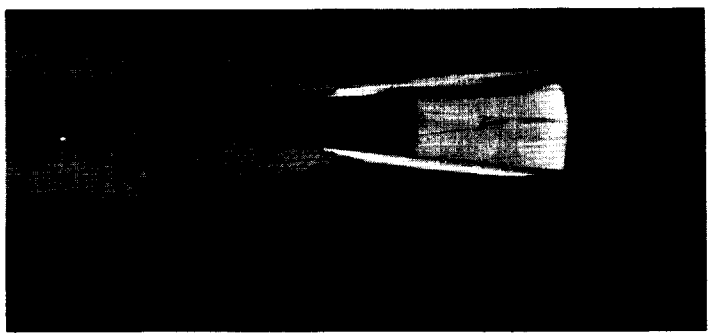

(b) $\alpha = 6^\circ$; d/c = 0.16; V = 164.19 fps.

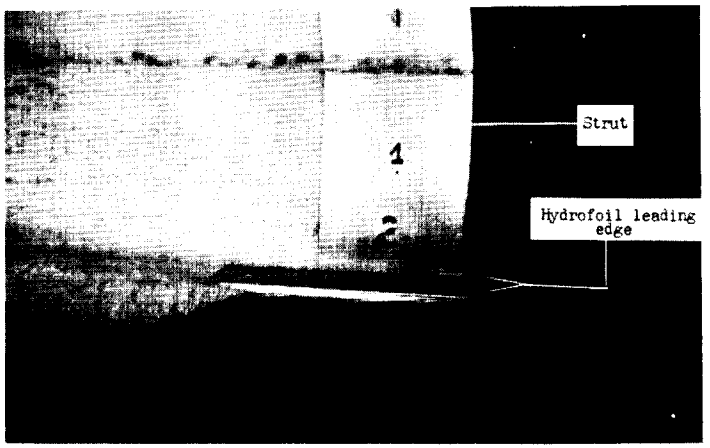

(c) $\alpha = 9^\circ$; d/c = 0.7 (estimated); V = 184.28 fps.

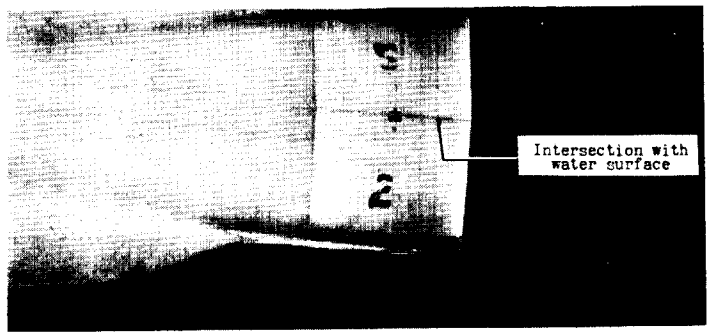

L-60-2440

(d) $\alpha = 9^\circ$; d/c = 0.38; V = 153.70 fps.

Figure 7.- Photographs of the flow about the aspect-ratio-1 hydrofoil at various depths and angles of attack.

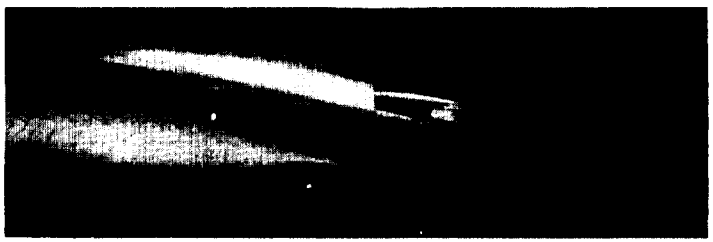

Overhead camera

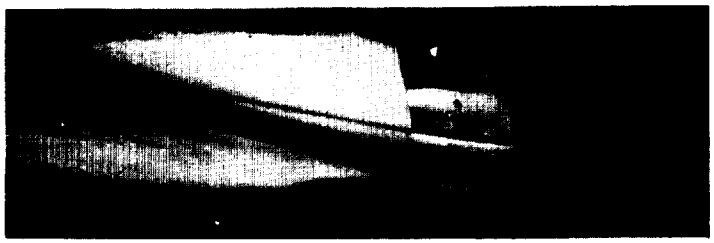

Overhead camera

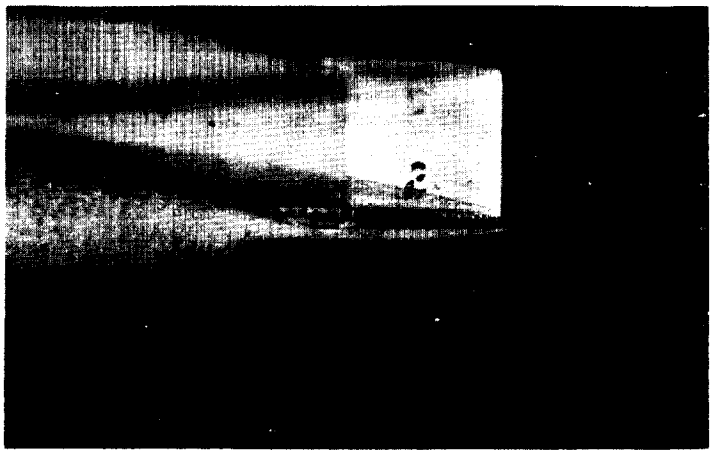

Underwater camera

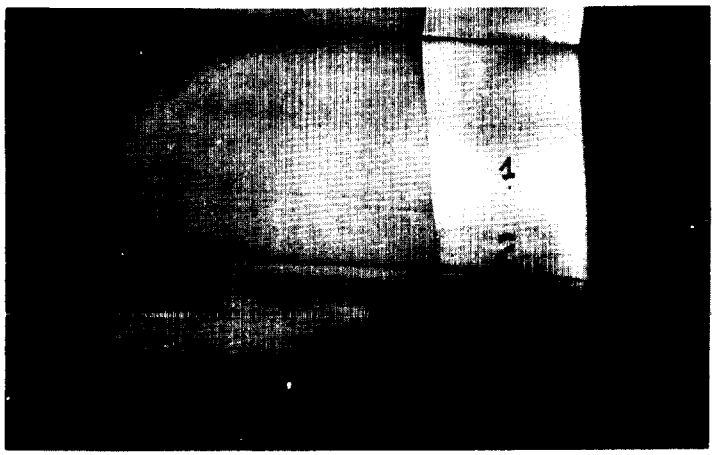

Underwater camera

L-60-2441

(e) $\alpha = 12^{\circ}$; d/c = 0.25; V = 182.89 fps.

(f) $\alpha = 16^{\circ}$; d/c = 0.85 (estimated); V = 166.27 fps.

Figure 7.- Concluded.

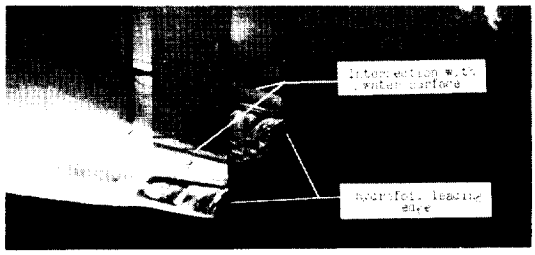

(a) $\alpha = 8^{\circ}$; $d/c = 0.51$;
$V = 150.37$ fps.

(b) $\alpha = 9^{\circ}$; $d/c = 0.7$ (estimated);
$V = 158.08$ fps.

(c) $\alpha = 14^{\circ}$; $d/c = 0.49$;
$V = 127.69$ fps; overhead camera.

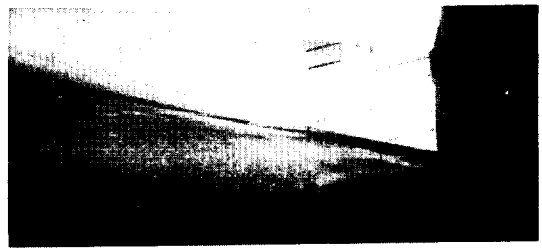

(d) $\alpha = 14^{\circ}$; $d/c = 0.49$;
$V = 127.69$ fps; underwater camera.

(e) $\alpha = 14^{\circ}$; $d/c = 0.47$;
$V = 138.64$ fps; overhead camera.

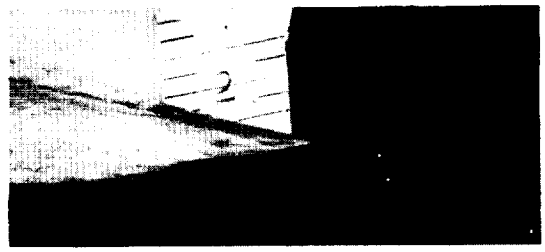

L-60-2442

(f) $\alpha = 14^{\circ}$; $d/c = 0.47$;
$V = 138.64$ fps; underwater camera.

Figure 8.- Photographs of the flow about the aspect-ratio-3 hydrofoil at various depths and angles of attack.

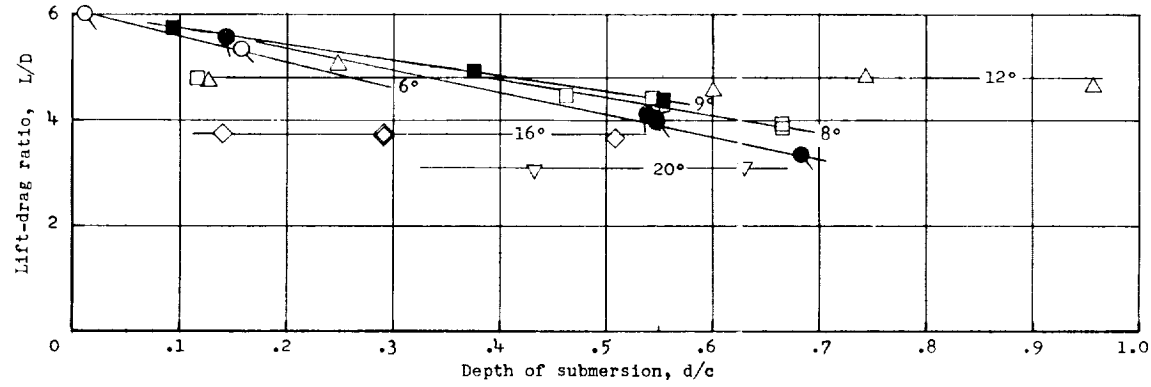

(a) Aspect-ratio-1 hydrofoil.

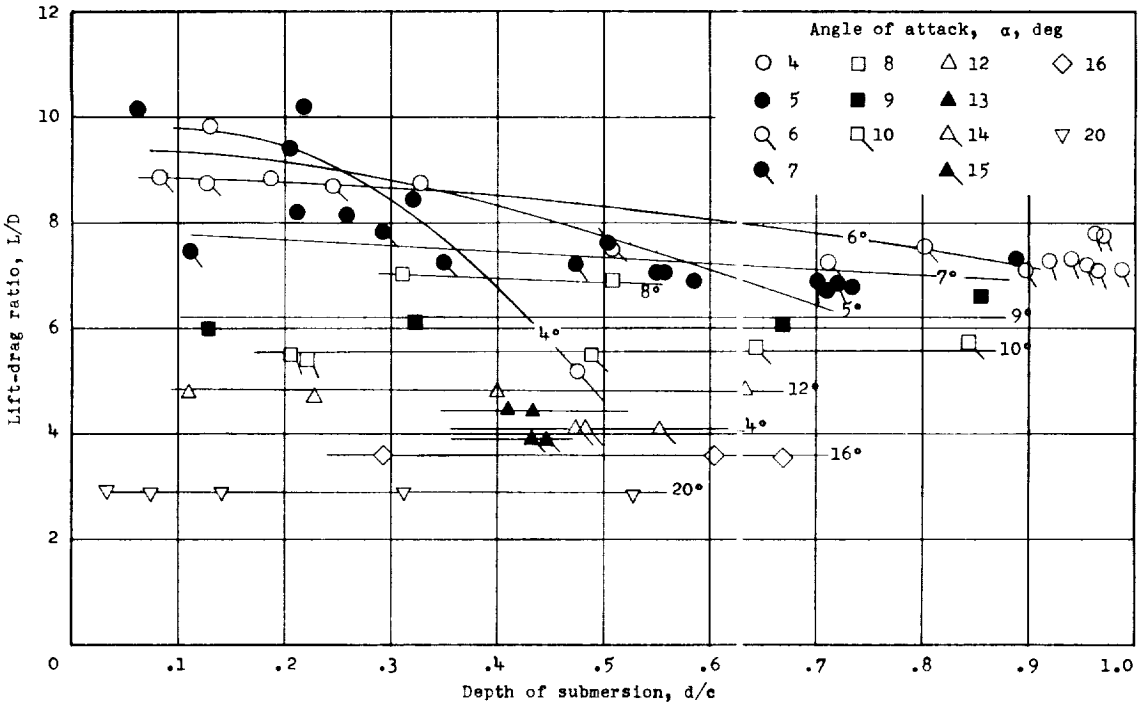

(b) Aspect-ratio-3 hydrofoil.

Figure 9.- Variation of lift-drag ratio with depth of submersion.

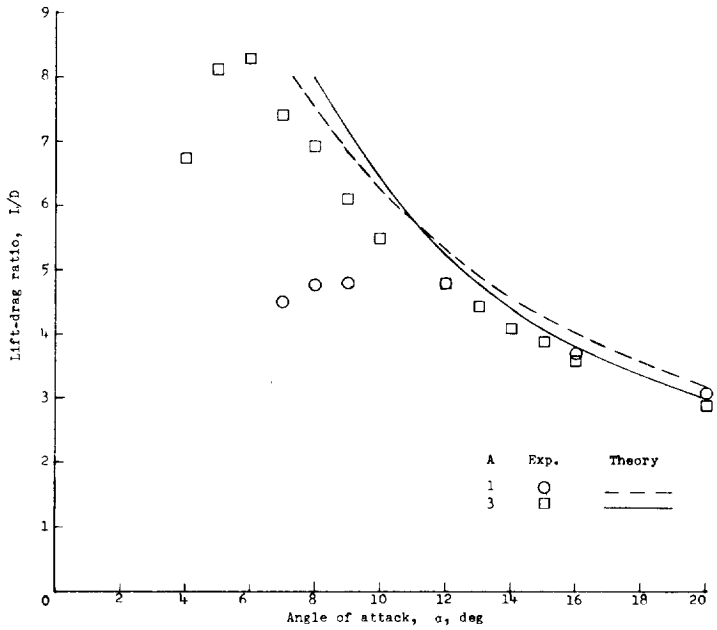

(a) Variation of lift-drag ratio with angle of attack.

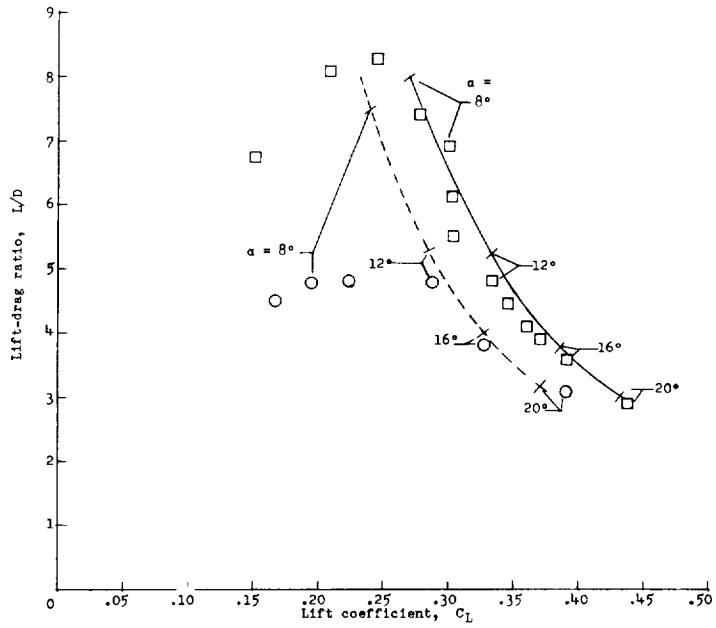

(b) Variation of lift-drag ratio with lift coefficient.

Figure 10.- Variation of lift-drag ratio with angle of attack and lift coefficient at constant depth of submersion. d/c = 0.4.

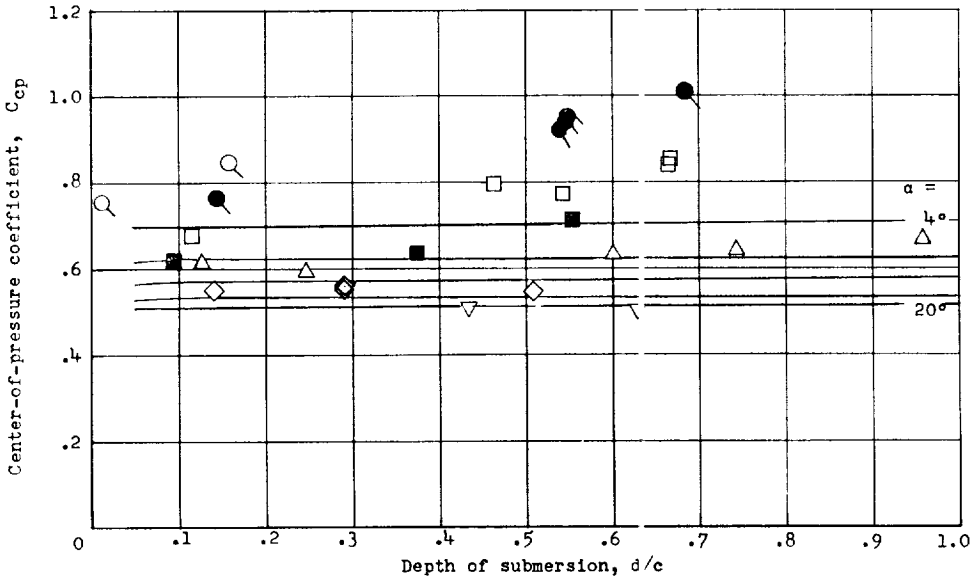

(a) Aspect-ratio-1 hydrofoil.

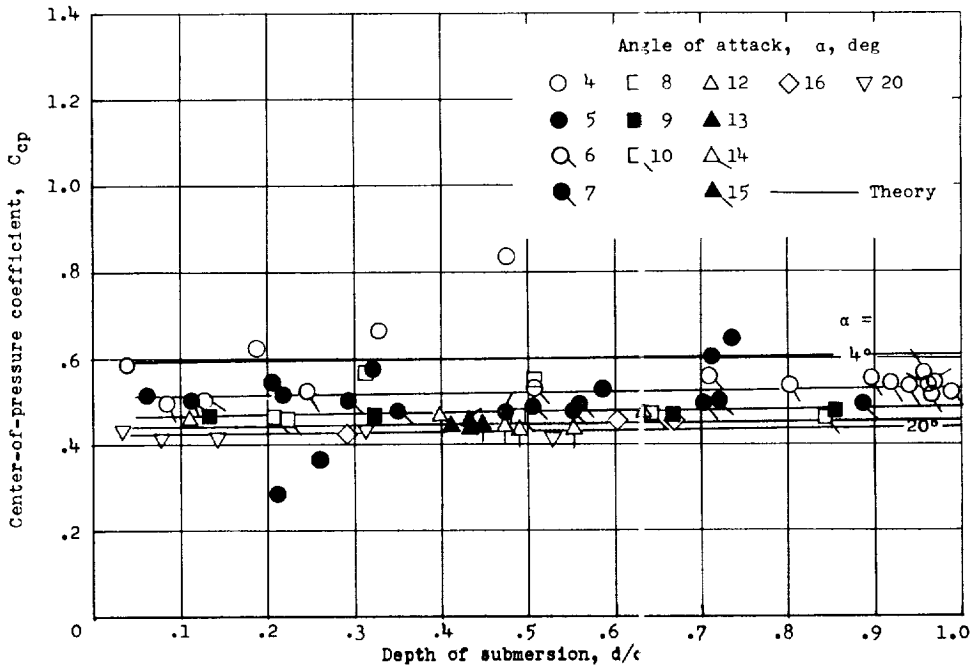

(b) Aspect-ratio-3 hydrofoil.

Figure 11.- Variation of center-of-pressure coefficient with depth of submersion.

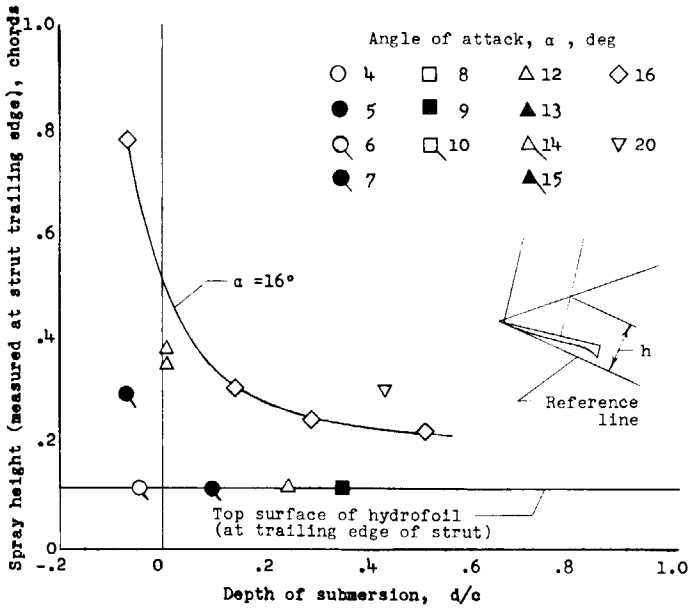

(a) Aspect-ratio-1 hydrofoil.

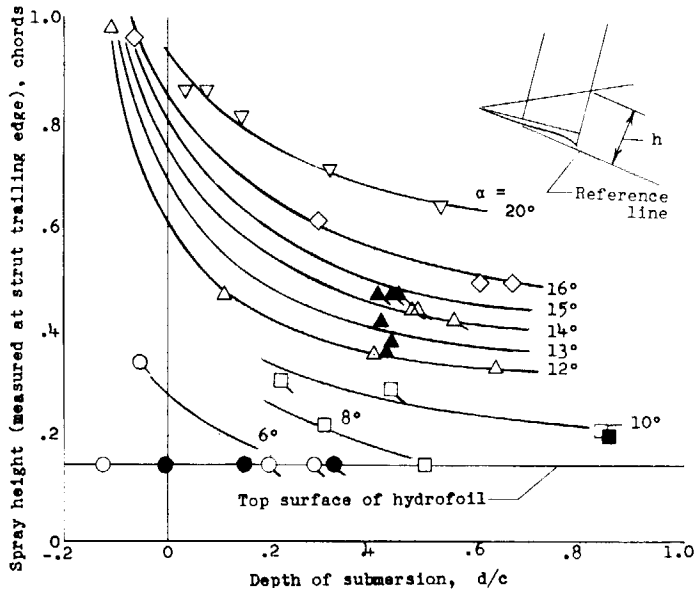

(b) Aspect-ratio-3 hydrofoil.

Figure 12.- Variation of experimental values of spray height with the depth of submersion.

(a) d/c = 0.41 (estimated); V = 188.82 fps.

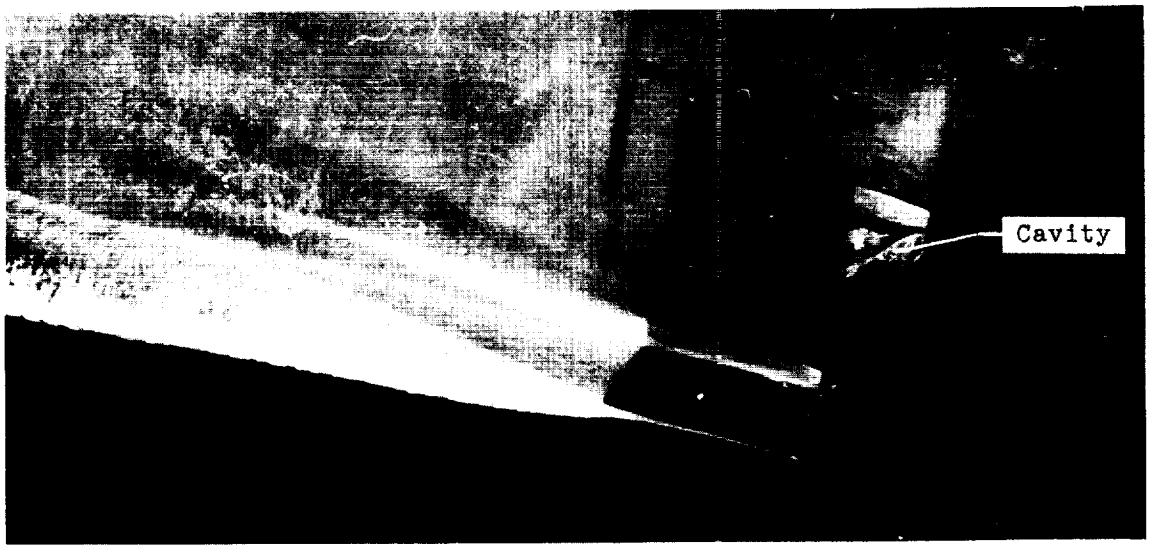

(b) d/c = 0.16 (estimated); V = 191.68 fps. L-60-2443

Figure 14.- Photographs of the flow about the aspect-ratio-3 hydrofoil at $\alpha = 4^{\circ}$.

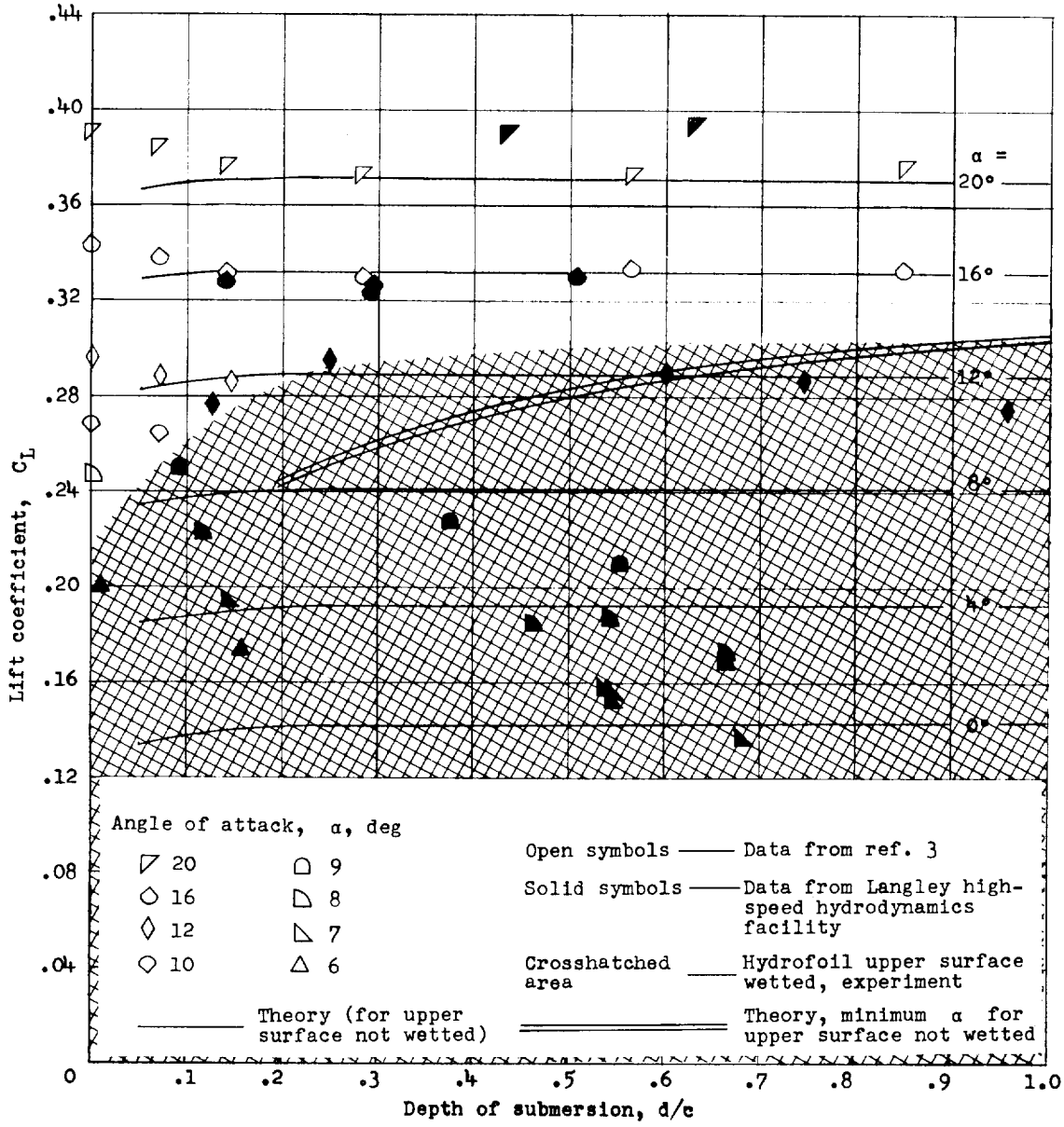

(a) Aspect-ratio-1 hydrofoil.

Figure 15.- Comparison of present lift data with data obtained at low speeds (ref. 3).

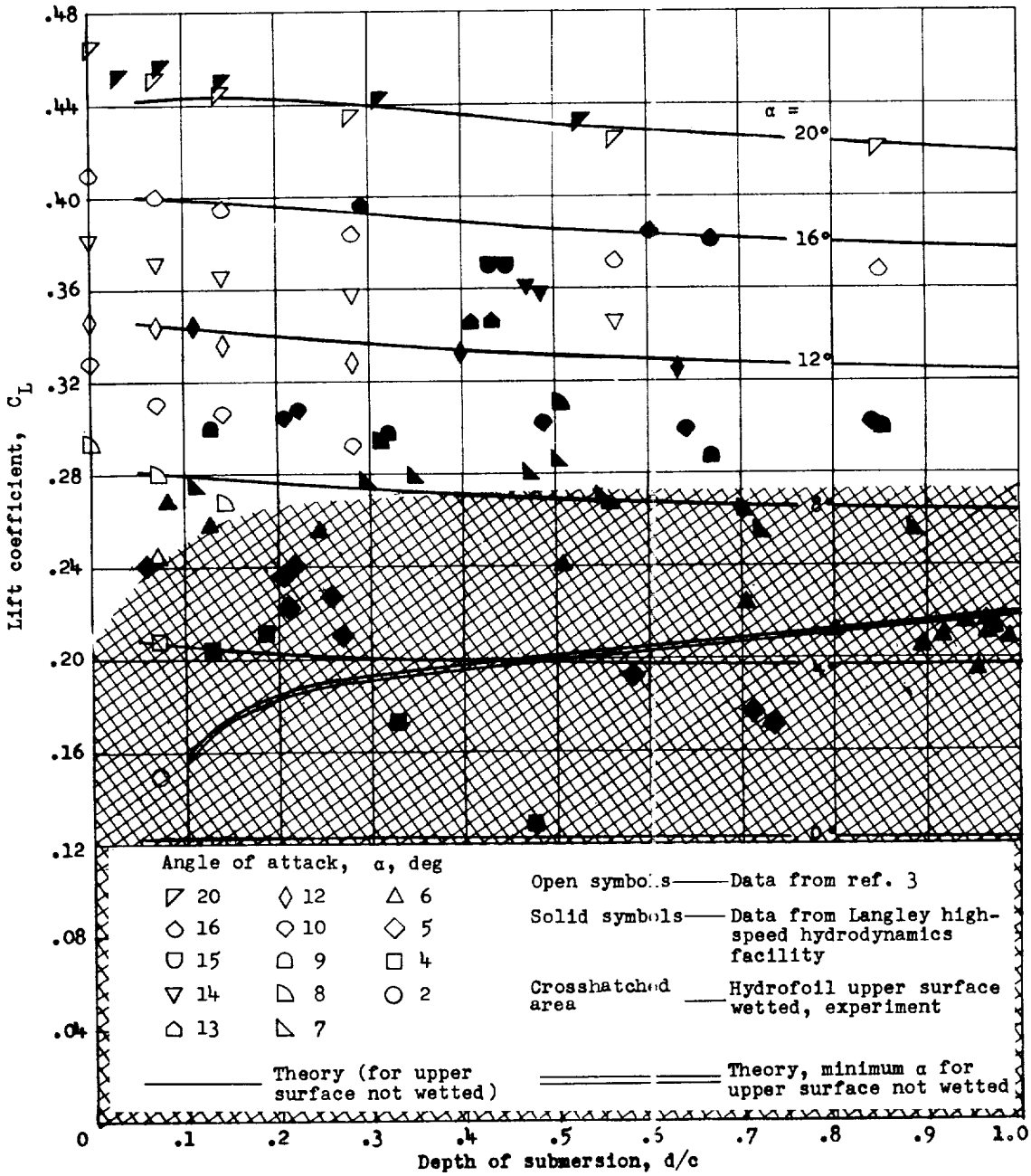

(b) Aspect-ratio-3 hydrofoil.

Figure 15.- Concluded.

L-913